Kinetics of alloy formation at the interfaces in a Ni-Ti multilayer: X-ray and neutron reflectometry study

Surendra Singh,[1] Saibal Basu,[1] Pramod Bhatt,[2] and A. K. Poswal[3]
[1]*Solid State Physics Division, Bhabha Atomic Research Center, Mumbai-85, India*
[2]*Department of Science and Technology, Linköping University, SE-601 74, Norrköping, Sweden*
[3]*Spectroscopy Division, Bhabha Atomic Research Center, Mumbai-85, India*
(Received 24 November 2008; revised manuscript received 20 March 2009; published 28 May 2009)

Vacuum-deposited Ni/Ti multilayers on annealing at different temperatures exhibit formation of ordered alloy layers at interfaces. We have studied in detail the formation of alloy at interfaces of a Ni/Ti multilayer on annealing at 300 °C and 400 °C using powder x-ray diffraction, x-ray reflectometry, polarized neutron reflectometry, and off-specular x-ray reflectometry techniques. Correlation among structural, magnetic, and morphological properties in as-deposited Ni/Ti multilayer as well as in a sample annealed at 300 °C and 400 °C has been studied. X-ray diffraction technique was used to obtain crystal structure of the sample. Specular x-ray reflectometry and neutron reflectometry were used to determine the growth of alloy layers from density profile, as a function of depth in the sample. From off-specular x-ray reflectivity we found that the in-plane correlation lengths at the interfaces grew with annealing. This is associated with alloy crystallite growth obtained from x-ray reflectometry. Detailed magnetic-moment density profile of as-deposited as well as annealed multilayer sample has been determined by polarized neutron reflectometry measurements, which was used to determine the magnetic nature of the alloy layers. The results show formation of nonmagnetic alloy layers at the interfaces on annealing. From the Bragg-peak intensities of x-ray reflectivity and polarized neutron reflectivity measurements, we have estimated the diffusion lengths after annealing at 300 °C and 400 °C.

DOI: 10.1103/PhysRevB.79.195435 PACS number(s): 61.05.fj, 61.05.cm, 75.70.−i

I. INTRODUCTION

Ni/Ti multilayers have been studied extensively as ideal candidates for neutron optics components, such as highly reflecting mirrors, supermirrors, polarizers, monochromators, etc.,[1–4] because they have an excellent contrast factor for thermal and cold neutrons. Ni-Ti alloys prepared by thin-film root showed interesting shape memory and super elastic effects.[5,6] These have been utilized to develop different micro electromechanical systems (MEMS) such as cantilevers, actuators, etc. Multilayers of Ni and Ti can be classified as composition-modulated structures.[7] Alloying of Ni/Ti at their interfaces in such composition-modulated samples shows various interesting behavior.[7,8] Clemens[7] found that as one goes from large modulation length (200 atomic planes per layer) to shorter modulation length (2 atomic planes), the structure changes from crystalline to amorphous in Ni/Ti alloys. Recently Gupta *et al.*[8] studied alloying at the interfaces in Ni/Ti multilayers. They observed that the alloying at the interfaces produces amorphous phase, which justifies the slowing down of alloying as a function of annealing temperature in their studies. In another study Bhatt *et al.*[9] also found that the alloying in Ni/Ti multilayers of modulation length 10 nm [Ti 5 nm+Ni 5 nm] undergoes amorphization at the interfaces through a solid-state reaction. A large number of studies exists which show that at intermediate and shorter modulation wavelengths alloying at the interfaces of Ni and Ti progress through amorphization. Formation of an amorphous phase on annealing arises due to large asymmetry in the atomic mobility of the constituents of the system and their large negative Gibbs free energy of mixing. It has also been indicated that the presence of certain degree of disorder (e.g., roughness, etc.) at the interface of an as-deposited sample facilitates the growth of amorphous layer at the interface on annealing. Interface quality, which gets modified on annealing, is an important parameter that can also influence the above-mentioned technological applications of the Ni/Ti multilayers. Interface morphology plays a vital role for nucleation and growth of multilayers and subsequently the structural and magnetic properties of the system. In the present work, we have found that contrary to the previous observations, alloying at the interfaces of Ni/Ti multilayer samples may also progress through the formation and growth of microcrystals at the interfaces. We had prepared Ni/Ti multilayers of various modulation lengths on glass substrate by vacuum deposition. The samples were annealed first at 300 °C and then at 400 °C for a fixed time of 1.5 h. We found that in several samples annealing produces crystalline phases at the interfaces during annealing and the grains have grown with annealing temperature, unlike the growth of amorphous phase discussed in previous studies. Growth of the microcrystallites was confirmed from narrowing of x-ray powder diffraction (XRD) lines. Thickness and density of interface layers have been obtained from x-ray reflectometry (XRR) and neutron reflectometry (NR). Apart from the physical density change at the interfaces, we have confirmed the formation of magnetic dead layers at the interfaces by polarized neutron reflectometry (PNR), which belong to the possible alloy phases Ni_3Ti or NiTi. Structural and magnetic properties of artificial multilayered systems are strongly influenced by growth conditions and subsequent thermal treatment.[10] We have estimated the diffusion constants from XRR and NR density data taken after annealing the sample at 300 °C and 400 °C. From these *snap-shot* density profiles after each anneal and from the XRD data, we observe that there is a sharp rise in the diffusion constant and increase in

the size of alloy crystallites in the present sample as a function of annealing temperature. Further, the growth in crystallite size with annealing is associated with increase in the correlation length at the interface. This has been confirmed using off-specular x-ray reflectivity from the as-deposited and annealed sample. Morphology of the interface and particularly its roughness parameters play a major role for global electronic, magnetic, transport, and optical properties[11] in such multilayer samples.

II. EXPERIMENTAL DETAILS

Ni/Ti multilayer structures were deposited on float glass substrates using electron beam (e-beam) evaporation technique under ultra-high-vacuum conditions at room temperature. In order to avoid contamination during deposition, the system was thoroughly baked at a temperature of 200 °C for 12 h to achieve a background pressure of 5×10^{-10} Torr. Deposition of both Ti and Ni layers was carried out at a rate of 0.1 Å/s. For all the samples, first a Ni layers of thickness ~50 Å was grown on float glass substrate. Then a Ti layer of thickness ranging from 50 to 70 Å was grown. Ten such bilayers were deposited for all the samples. A thin layer of 20 Å of carbon was deposited as a protective cap layer at the air-film interface. The designed structure of the multilayer sample on which detailed XRR and PNR were carried out can be represented as float glass substrate/$[\mathrm{Ni}_{50\ \text{Å}}/\mathrm{Ti}_{50-70\ \text{Å}}]\times10/\mathrm{C}_{20\ \text{Å}}$. The layer thicknesses were decided based on the fact that the samples should grow in crystalline phase in these compositionally modulated samples,[7] since the aim of the present study was to track alloy formation at the interfaces through crystalline route. During deposition, thickness of each layer was monitored using a water-cooled quartz-crystal thickness monitor. The sample was annealed at temperatures of 300 °C and 400 °C for 1.5 h under a high vacuum of the order of 1×10^{-6} Torr after performing experiments with the as-deposited sample.

The crystalline structure of as-deposited as well as annealed multilayer sample was investigated using XRD with Cu K_α x rays. NR and XRR are nondestructive tools that are routinely used for obtaining the depth profile of densities in thin-film samples.[12–17] They are capable of providing density as a function of depth in a film with resolution as low as 0.1 nm. The microstructure parameters, i.e., thickness, density of each layer, and interface roughness in the sample were determined by XRR as well as by NR. In order to determine the magnetic-moment density in various layers of the films, PNR measurements were performed. NR experiments were carried out at polarized neutron reflectometer instrument at Dhruva, India.[18] We have also obtained the change in the morphology at the interfaces of the sample due to alloying, from off-specular or diffuse x-ray reflectivity.

III. RESULTS AND DISCUSSION

A. Crystalline structure from x-ray diffraction

Figures 1(a)–1(c) show XRD patterns recorded from as-deposited as well as annealed Ni/Ti multilayer sample S1 (ten bilayers of Ni 50 Å+Ti 70 Å on glass substrate). The

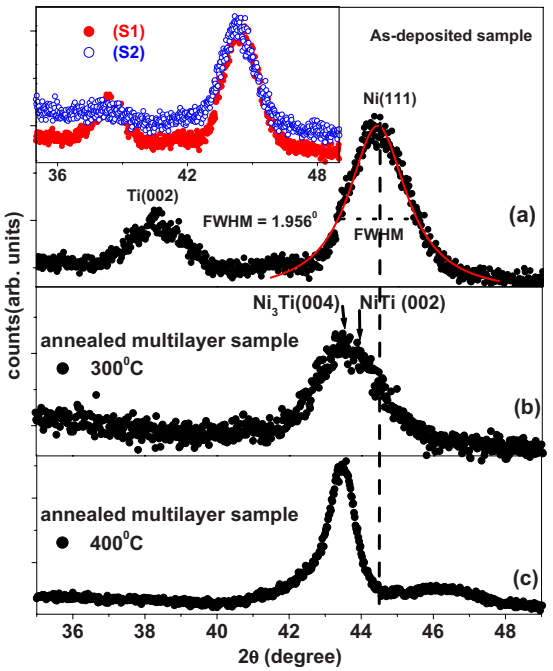

FIG. 1. (Color online) (a) X-ray diffraction pattern of Ni/Ti multilayer sample from as-deposited, (b) after annealing at 300 °C, and (b) at 400 °C. (a) The solid line corresponding to Ni (111) peak in is a Lorentzian fit to the XRD data, which gives a full width of half maxima (FWHM)=1.956°. Inset of Fig. 1(a) shows the XRD pattern from as-deposited Ni/Ti multilayer samples S1 and S2 with different modulation length.

inset of Fig. 1(a) shows the XRD patterns of two as-deposited Ni/Ti multilayers, S1, and S2 (ten bilayers of Ni 50 Å+Ti 50 Å), respectively, each having ten bilayers of Ni and Ti with different Ti layer thicknesses. Both the as-deposited samples show two peaks at 2θ values of 38.4° and 44.5°. These peaks can be attributed to hcp Ti (002) (38.4°) and fcc Ni (111) (44.5°), respectively. This confirms that the Ni and Ti layers are crystalline in these multilayer samples. Only the Ni (111) diffraction peak with a lattice spacing of $d_{\mathrm{Ni}}(111)=2.034$ Å was observed for Ni in all the multilayers. This is due to the fact that the Ni layers had grown with a strong [111] texture. Similarly the Ti layers grew with a (002) texture along the normal to the surface of the film. In both S1 and S2, between these two peaks, the Ti peaks are more diffuse compared to Ni. It indicates that though the Ti layers are crystalline, the grain sizes are smaller and they are more disordered compared to the Ni layers. The sample S1 shows best the crystalline nature for both Ni and Ti layers and we have carried out detailed XRD, XRR, and PNR works on this sample after annealing at 300 °C and 400 °C.

Size of crystallites, t can be calculated from the peak widths in XRD. The Scherrer formulation relates the crystallite size t to the angular broadening B (in radians) at the Bragg reflection θ_B as[19]

$$t=\frac{0.9\lambda}{B\cos\theta_B}, \tag{1}$$

where λ is the x-ray wavelength. Using the above equation we have estimated the crystallite size of Ni from the (111)

Bragg reflection. The crystallite size of Ni, t_{Ni}, is 45 Å for the full width at half maximum (FWHM) (B)=1.956° at Ni (111) Bragg reflection. This is close to the design thickness of the Ni layers (50 Å) obtained from XRR and NR data. This shows that for the Ni layers the grain size and the layer thicknesses are of the same order in the as-deposited sample.

Figures 1(b) and 1(c) give the XRD pattern of the sample S1 after annealing at 300 °C and 400 °C, respectively, which shows a noticeable change with respect to the as-deposited XRD pattern. These changes are (i) a prominent shift of the Ni (111) peak by about 1.0° to a lower angle of 43.6° and (ii) an increase in the peak width, for a sample annealed at 300 °C. The shift in the peak position and increase in its width, for a sample annealed at 300 °C, have been confirmed in repeated XRD runs. Hollanders *et al.*[19] suggested small shift (~0.1°–0.6°) of Ni peaks toward low angle due to the competition between compositional homogenization of the Ni sublayer and coherency strains in Ni, induced by dissolution of Ti in Ni. This angular shift of the peak at 44.5° is large (~1°) and any shift in peak position due to strain cannot explain such a large shift of 1°. The broadening of the peak also points to a possibility of overlap of number of peaks. Close to Ni [111] peak at 44.5°, the [004] peak of Ni_3Ti at 43.69° and NiTi (002) peak at 44.0° are distinct possibilities. The broad peak also shows a hump at the previous position of the Ni peak at 44.5°. We have fitted two Lorentzian peaks for the shifted peak, one centered at 43.6° and the other centered at 44.5°. From the width of the peak centered at 43.6° we obtained an average grain size of nearly 48 Å for the alloy crystallites. Figure 1(c) for the sample annealed at 400 °C shows a distinct narrowing of this peak. There is a well-defined crystalline peak around 2θ of 43.6°, which corresponds to the [004] peak of ordered Ni_3Ti alloy phase. The disappearance of the Ti peak and a broad peak after the first anneal at 300 °C was followed by the narrowing of the same broad peak on further annealing at 400 °C. This indicates the growth of a crystalline alloy layer at the cost of Ni and Ti layers in the sample. The narrowing of the diffraction peak after annealing at 400 °C is a clear signature of an increase in the size of alloy crystallites. From the Debye-Scherer relation we obtain a grain size of ~100 Å for these alloy crystallites. The XRD data indicate that in the present sample the alloying at the interface propagates through the crystalline route. We have quantified the thickness and density of the alloy layers in the sample from XRR and NR data. In the case of the Ti/Ni multilayer structure, Ni atoms are more mobile and would start diffusing into the relatively immobile lattice of Ti layers. We will show later from our XRR and NR that this asymmetry in diffusion leads to asymmetric thickness of the alloy layers at the interface for Ni on Ti with respect to Ti on Ni.

B. Specular x-ray and neutron reflectometry

Neutron and x-ray reflectometry[12–17] are nondestructive tools which provide magnetic and chemical depth resolutions as low as 0.1 nm. Specular reflectivity from a sample is measured as a function of the wave vector transfer Q [$Q=(4\pi/\lambda)\sin\theta$, where θ is the incident angle on the film and λ is the wavelength of the probe]. The reflectivity depends on the contrast in refractive index between layers of a film. A generic expression for refractive index for neutrons and x-rays can be given by[12,13]

$$n = 1 - (\alpha - i\beta). \tag{2}$$

In the case of neutrons

$$\alpha = \frac{\lambda^2}{2\pi}\sum_i N_i b_i^{\mathrm{coh}} \quad \text{and} \quad \beta = \frac{\lambda^2}{2\pi}\sum_i N_i b_i', \tag{3}$$

where λ is the wavelength of neutron and b_i^{coh} is the coherent scattering length for the neutron-nucleus interaction for species i and b_i' is the absorption length for neutrons the species i. For most of the samples, neutron absorption coefficient is negligibly small. N_i is the number density of scatterers per unit volume (averaged over sample surface), which is connected to the physical density. In the case of x rays,

$$\alpha = \frac{\lambda^2 r_0}{2\pi}\sum_i N_i(Z_i + f_i') \quad \text{and} \quad \beta = \frac{\lambda^2 r_0}{2\pi}\sum_i N_i f_i'', \tag{4}$$

where Z_i is the atomic number of the ith species, r_0 is the classical electron radius (=2.818 fm), f_i' is the real anomalous dispersion factor, and f_i'' is the absorption coefficient of the species for x rays. The scattering length density for neutron is given by $\Sigma_i N_i b_i^{\mathrm{coh}}(=\rho_n)$ and that for x rays is given by $\Sigma_i N_i r_0(Z_i+f')(=\rho_{\mathrm{xray}})$. The difference between these two values is the reason for a medium to have different refractive indices with respect to x rays and neutrons. We have obtained the coherent scattering length densities, ρ_n, and electron scattering length densities (ESLD), ρ_{xray}, from NR and XR data as functions of depth in the Ni-Ti film in units of $Å^{-2}$. The element Ti has b^{coh} values negative for thermal neutrons (−3.45 fm), while Ni has a positive coherent scattering length of 10.3 fm.[20] Due to this reason Ni and Ti provide excellent contrast in neutron reflectometry. Also the values of ρ_n and ρ_{xray} obtained from the fits to both XRR and PNR data have allowed us to derive the stoichiometry in the interface alloy region as we show later. In addition to the scattering length density profile, interface roughness at different interfaces is an important parameter, which can be extracted from the analysis of XRR and NR measurements.[12–17] Roughness has the effect of reducing the specularly reflected intensity and the fitting program takes into account the reduction in specular intensity by introducing a multiplicative exponential factor, as proposed by Nevot and Croce[21] and given by

$$r_j^m = r_j^0 e^{-4 q_j q_{j-1} \sigma_j^2}, \tag{5}$$

where σ_j and q_j are the root-mean-square roughness amplitude and the perpendicular wave vectors in the jth interface. r_j^o is the Fresnel intensity reflection coefficient for a perfectly smooth interface, and r_j^m is the measured specular intensity from a sample with rough interfaces. This multiplicative "Debye-Waller-type" factor is due to the uncertainty in location of the interface due to (a) jaggedness at the interface and (b) continuous change in density across the interface. The roughness amplitude σ_j is a convolution of both these ef-

fects. The role of roughness toward the modification of an ideal ESLD in the present samples has been discussed later.

In the case of magnetic materials the depth profile of scattering length density ($\rho_n(z)$) for polarized neutrons has both a nuclear component (ρ_{nuc}) dependent on the coherent scattering lengths b^{coh} of the constituent elements and a magnetic component (ρ_{mag}).[16,17] The sign of the magnetic part depends on the polarization of the sample with respect to polarization direction of neutron beam. Specifically, the polarized neutron reflectivity can be fitted[12–17] using a depth-dependent scattering length density (SLD) profile $\rho_n(z)$ with nuclear and magnetic components,

$$\rho_n(z) = \rho_{\text{nuc}}(z) \pm \rho_{\text{mag}}(z), \quad \rho_{\text{nuc}}(z) = \sum_i N_i(z) b_i,$$

$$\rho_{\text{mag}}(z) = C \sum_i N_i(z) \mu_i, \tag{6}$$

where the summation is over each type of atom in the system, $N(z)$ is the depth-dependent number density, b^{coh} is the nuclear scattering length, and μ is the magnetic moment of the scatterer atom in Bohr magnetons. The constant $C = 2.69$ fm/μ_B. The sign before ρ_{mag} in Eq. (6) depends on the orientation of the magnetization relative to the neutron polarization and correspondingly we get two reflectivity patterns for two spin of neutrons, i.e., spin up (+), parallel to sample magnetization and spin-down neutron (−), antiparallel to sample magnetization. NR and XRR are complementary techniques for measuring the depth profile of density in Ni/Ti multilayer systems. NR is quite sensitive in this system because of higher contrast between Ni and Ti (ρ_{nuc} for Ni and Ti are 9.4×10^{-6} Å^{-2} and -1.95×10^{-6} Å^{-2}, respectively) while for Cu K_α, ρ_{xray} for Ni and Ti are 6.42×10^{-5} Å^{-2} and 3.55×10^{-5} Å^{-2}, respectively. In addition PNR is also sensitive to the depth profile of the magnetic-moment density (ρ_{mag} for Ni is 1.47×10^{-6} Å^{-2} and for Ti it is zero). Using these two probes in the present set of studies we have accurately estimated the compositional depth profile of Ni/Ti multilayers on annealing. In addition, by using PNR measurements, we have determined the extent of alloying at Ni/Ti interfaces on annealing at temperatures 300 °C and 400 °C by tracking the magnetic-moment density of the alloy layers. Especially the possible alloy compositions, i.e., Ni_3Ti and NiTi are both nonmagnetic and provide excellent contrast with respect to magnetic Ni layers.

Figure 2 shows the XRR data of as-deposited multilayer S1 (closed circles) as well as the sample annealed at 300 °C (open circles) and 400 °C (open squares) along with the corresponding fits (continuous lines) to the measured data. The XRR pattern of the as-deposited multilayer sample shows Bragg peaks up to the fifth order. The thicknesses for Ti and Ni layers are 66 and 54 Å, respectively, in the as-deposited sample. The roughness parameters for Ni/Ti and Ti/Ni interfaces, obtained from XRR measurements, are 9 ± 1 Å. There are several broad changes in the sample on annealing. After annealing at 300 °C (i) the second and the fourth order Bragg peaks have drastically reduced in intensity compared to the peaks of odd order, (ii) the slope of the reflectivity curve has increased beyond the critical angle, indicating that

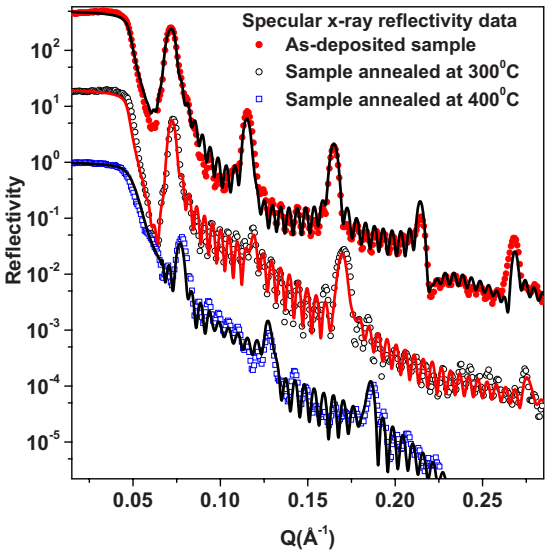

FIG. 2. (Color online) X-ray reflectivity pattern for as-deposited (closed circles) Ni/Ti multilayer sample and sample annealed at 300 °C (open circles) and 400 °C (open squares). While continuous lines are fits to the corresponding measured data.

the interlayer roughness in the film has increased, and (iii) the Bragg peaks have shifted to larger Q values. This shift is due to the release of strain, causing overall reduction in the bilayer thickness. The suppression of the even order Bragg peaks is due to the change in the individual layer thickness in the bilayers. After annealing at 300 °C, we find that the thickness of Ni-Ti alloy+Ti layers and that of Ni+Ni-Ti alloy are almost the same (~60 Å) within error bars. It is known that when the individual layer thicknesses are equal in a bilayer the even order Bragg peaks will be absent. To understand the microscopic change in details, we have fitted the XRR data from as-deposited and the annealed sample. In this case the changes are associated with the thickness and density of the interface alloy layers with respect to the as-deposited sample. The model that has been used to fit the data is shown in Figs. 3(a) and 3(b). Figure 3(a) shows the as-deposited sample with two Ni and Ti layers of uniform density. After annealing it was necessary to account for the two alloy layers at the interfaces as shown in Fig. 3(b). The alloy layers have distinctly different densities compared to the as-deposited layers. We have tracked the ESLD and thickness of the alloy layers at the interfaces using XRR. Figure 4 shows the ESLD in the sample in units of Å^{-2} as a

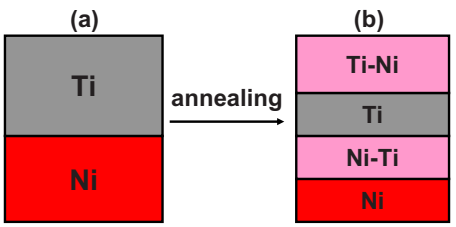

FIG. 3. (Color online) (a) Schematic of models of Ni/Ti bilayer, used for analyzing the X-ray and polarized neutron reflectometry data for as-deposited and (b) annealed samples at 300 °C and 400 °C.

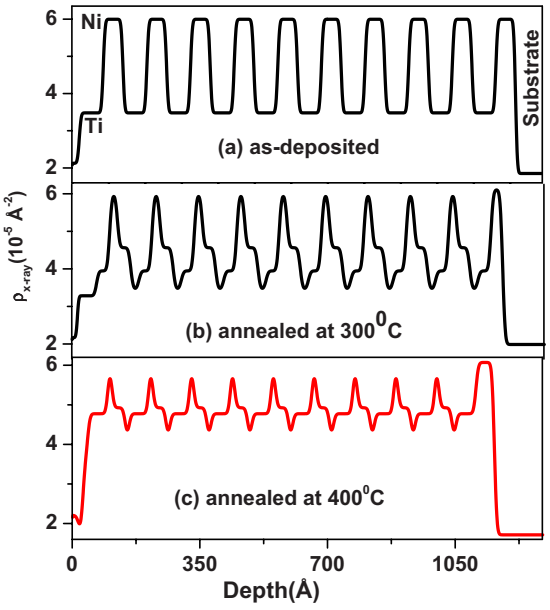

FIG. 4. (Color online) (a) Electron scattering length density depth profile for as-deposited, (b) Ni/Ti multilayer sample as well as sample annealed at 300 °C, and (c) 400 °C extracted from the x-ray reflectivity measurements.

function of depth. For generating the ESLD we have used the program PARRATT32,[22] which uses an error function to generate the density gradient at the interfaces. The width of the error functions are the roughness parameters (σ) obtained from the multiplicative Debye-Waller-type factor [Eq. (5)]. Table I gives the ESLD and thickness of layers for the as-deposited sample and for the sample after annealing. The values quoted in Table I are the average values for the respective layers in the multilayer. The as-deposited sample had Ni and Ti layer thickness 54 and 66 Å, respectively. After the first anneal there were distinctly two alloy layers of ESLD, $4.86 \pm 0.20 \times 10^{-5}$ and 4.20 ± 0.15 Å^{-2}, at the two interfaces between Ni and Ti [Table I, Fig. 4(b)]. The alloy layers at the interfaces have grown at the cost of Ni and Ti layers. After the second anneal at 400 °C we found from the XRR fit that the Ti layer was only 10 Å thick and the Ni layer was 7 Å. Correlating this with the XRD data, we conclude that the apparent shift in the XRD peak after annealing at 300 °C and its narrowing after annealing at 400 °C were due to the formation and growth of crystalline alloy layers at the interfaces. The XRD peak at 43.6° belongs to either Ni_3Ti [004] or NiTi [002] phase. We also note that the interface roughness has increased from 9 to 12 Å after the second anneal, which is due to alloying at the interfaces. We have also carried out off-specular x-ray reflectivity to determine the true morphology at the interfaces through height-height correlation function. The results are discussed later. The increase in the interface roughness is apparent from the rapid drop of the reflectivity curve after annealing. The density of the alloy layers had an asymmetry in density after the first anneal at 300 °C, which vanished after the second anneal but the alloy layers have a large asymmetry in thickness at the two interfaces (40 Å for Ti on Ni and 51 Å for Ni on Ti). This is most likely due to the difference in diffusivity of Ni and Ti and grain size of the microcrystallites at the interfaces. A similar type of asymmetric nature of interfaces was also reported by Jankowaski[23] in high-resolution transmission electron microscopy and Auger electron spectroscopy (AES) studies carried out on Ti/Ni multilayer deposited by sputtering. The possible alloy compositions in this case are Ni_3Ti and NiTi. Since both the possible interface alloy compositions, i.e., Ni_3Ti and NiTi, are nonmagnetic, they show up as magnetically dead layers in PNR measurements.

C. Magnetic depth profile from PNR measurements

Figure 5(i) (left panel) shows the PNR data for spin-up (+) and spin-down (−) neutrons from the as-deposited as well as annealed multilayer sample. Closed and open circles in Fig. 5(i) are the experimental data points for (+) and (−) polarized neutrons from as-deposited sample (a), sample annealed at 300 °C (b) and 400 °C (c), respectively. The solid lines are the fits to the corresponding measured data. The + and − correspond to the spin polarization of the neutrons parallel or antiparallel to the magnetization of the sample, respectively. The difference in the reflectivity pattern of the sample for spin-up and spin-down neutrons is due to the difference in the step potential of the Ni layers for the spin-up and spins down neutrons [i.e., difference in SLD profile for two spins, Eq. (6)]. The PNR profile for the annealed sample shows a drastic reduction in the Bragg-peak intensity as well as a shift in the Bragg peak toward higher-Q value, similar to what we had observed in XRR for the annealed sample. The reduction in the intensity of the Bragg peaks is due to alloying at the interfaces. The loss of magnetic moment is evident in the merging of the critical edge for the R^+ and R^- in the annealed sample. For analyzing the PNR data we have used the same model for the physical density profile obtained from XRR pattern for annealed

TABLE I. Structural parameters [i.e., thickness (d) in Å and electron scattering length density (ρ) in 10^{-5} Å^{-2}] extracted from x-ray reflectometry data for as-deposited Ni/Ti multilayer sample and sample annealed at 300 °C and 400 °C. The errors on the parameters are less than 5%.

	Substrate		Ni		Ni/Ti		Ti		Ti/Ni		C	
	d	ρ_{xray}	d	ρ_{xray}	d	ρ_{xray}	d	ρ_{xray}	d	ρ_{xray}	d	ρ_{xray}
As-deposited		1.85	54	6.00			66	3.48			20	2.13
300 °C		1.90	20	6.00	36	4.20	24	4.04	37	4.86	19	2.17
400 °C		1.88	7	6.30	51	4.80	10	3.92	40	4.95	18	2.20

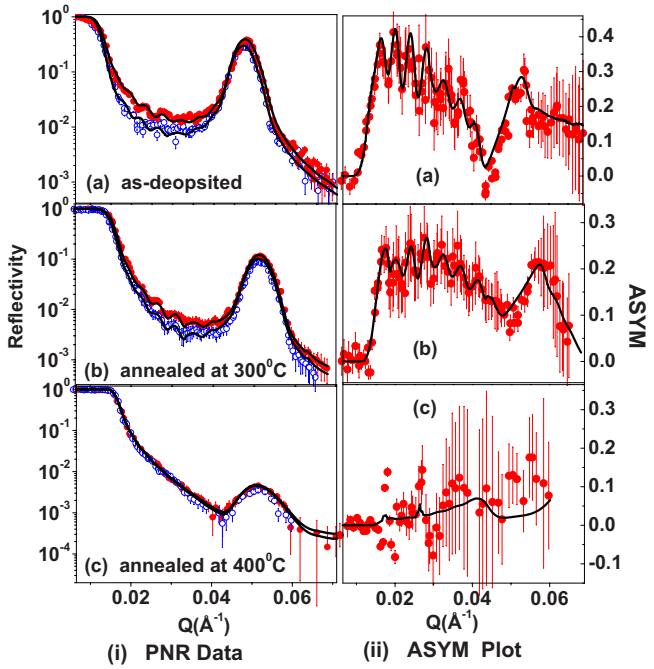

FIG. 5. (Color online) (i) Polarized neutron reflectivity pattern for as-deposited multilayer sample (a), annealed multilayer sample at 300 °C (b), and annealed multilayer sample at 400 °C (c). Closed circles and open circles are the experimental data for spin-up and spin-down neutrons whereas continuous lines are fit to the corresponding measured data for multilayer sample. (ii) The measured spin asymmetry (open circles) profiles for (a) as-deposited, (b) sample annealed at 300 °C, and (c) sample annealed at 400 °C, along with the fits (solid lines) from the corresponding SLD model.

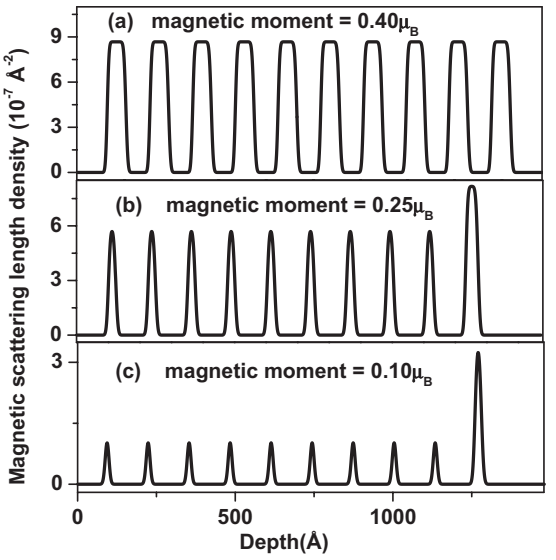

FIG. 6. The magnetic SLD depth profile for as-deposited (a) Ni/Ti multilayer samples as well as the sample annealed at (b) 300 °C and (c) 400 °C, as obtained from the PNR data.

sample. The structural parameters, viz., thickness, density, interface roughness, as well as the magnetic moment of the Ni layer, were the parameters of the fit. The structural parameters obtained from PNR and XRR measurements match within their experimental error bars. For every data set, i.e., as-deposited, sample annealed at 300 °C and sample annealed at 400 °C, we have also calculated the asymmetry (ASYM) function, which is defined as ASYM=$(R^+ - R^-)/(R^+ + R^-)$, where $R^{+(-)}$ are the spin-up (down) neutron reflectivity. The ASYM allows a direct comparison of the difference in the neutron reflectivities due to the spin-dependent magnetic interaction. The oscillations in the ASYM spectra are related to the layer thickness while the amplitude is related to the contrast between spin-up and spin-down neutron reflectivities. The ASYM parameter depends on the interface roughness to a much smaller extent compared to R^+ and R^-. The measured spin asymmetries and those from the fits to the reflectivity for the as-deposited (a), as well as the annealed multilayer sample at 300 °C (b) and 400 °C (c) are plotted together in Fig. 5 (right panel) along with R^+ and R^- (left panel). The peak amplitudes of the spin asymmetry at low Q are largely determined by the magnitude of the net magnetization of the magnetic layer in sample. The smearing of the oscillations in ASYM for the annealed samples is due to the gradual decrease in the magnetization upon annealing. After second anneal, the experimental data for R^+ and R^- almost merge, resulting in a smaller value of the ASYM parameter fluctuating around zero with large error bars [Fig. 5(c), right panel]. While some general trends can still be seen in the ASYM plot of Fig. 5(c), it is difficult to visualize any finer details. The magnetic scattering length density profile that gave best fit to PNR data for the as-deposited (a) and annealed multilayer sample at 300 °C (b) and 400 °C (c) has been shown in Fig. 6. It is clear that the nonmagnetic alloy layers at the interface grow at the cost of the Ti layer (nonmagnetic) and the Ni layers (magnetic). We also observe that as the thickness of Ni layers reduces, the magnetic moment per Ni atom goes down from $0.4\mu_B$ to $0.25\mu_B$ after annealing at 300 °C, which further reduces to $0.1\mu_B$ after the second anneal at 400 °C. This is a clear confirmation of the fact that nonmagnetic alloy layers are formed at the interfaces as a function of annealing. In addition, the interface roughnesses increase from the as-deposited sample to the annealed sample. The thickness of Ni and Ti layers reduces to ~7 Å after the second anneal at 400 °C and the fitted roughness is more than the layer thickness of Ni and Ti layers. This is also a consequence of alloying at the interfaces. The alloy layers are nearly 40 and 51 Å thick after the second anneal. PNR has confirmed that both the alloy layers are nonmagnetic. We found from XRD that these nonmagnetic alloys are possibly Ni_3Ti and NiTi crystallites. The parameters extracted from PNR measurements are given in Table II. For Ni layers we have given both nuclear and magnetic parts of SLD, whereas the magnetic SLD for other layers (nonmagnetic or magnetic dead layers) are zero. We have used the ρ_{nuc} and ρ_{xray} values, extracted from XRR and PNR measurements, for the interface region (Tables I and II) after the second anneal at 400 °C to obtain the Ni/Ti ratio in terms of their respective number densities. The volumetric ratio Ni:Ti is equal to 2.4:1. From this ratio, we conjecture that the interface alloy layer is possibly Ni_3Ti. The results of XRR and PNR have also allowed us to estimate the diffusivity of the elements at the interfaces, described in the next section.

TABLE II. Physical parameters obtained from PNR measurements of as-deposited as well as annealed multilayer sample at 300 °C and 400 °C. In the table d and ρ are the thickness (in Å) and scattering length density (in 10^{-6} Å^{-2}) of each layer. In case of Ni layer we have also obtained the magnetic scattering length density (ρ_m) measured in 10^{-7} Å^{-2}. For alloy layers at interfaces there is no magnetic contribution suggesting magnetic dead layers. The errors on parameters are less than 5%.

	Substrate		Ni			Ni/Ti		Ti		Ti/Ni		C	
	d	ρ_{nuc}	d	ρ_{nuc}	ρ_{mag}	d	ρ_{nuc}	d	ρ_{nuc}	d	ρ_{nuc}	d	ρ_{nuc}
As-deposited		3.15	55	8.78	8.40			70	−1.81			17	8.66
300 °C		3.19	22	8.69	5.90	40	2.53	23	−1.61	45	5.69	16	8.66
400 °C		3.30	6	8.10	2.30	51	5.61	9	−1.80	74	5.31	17	7.70

D. Diffusivity at interfaces

Another important aspect, which could be quantified from PNR and XRR reflectivity data, was the diffusivity of the constituent elements at the interfaces. The observed decay of the Bragg-peak intensities in XRR and PNR measurements from the sample annealed at 300 °C and 400 °C have been used to calculate the diffusivity of the constituent elements as well as the diffusion length at these annealing temperatures using the expression[24]

$$\ln[I(t)/I(0)] = -8\pi^2 n^2 D(T) t/d_{bl}^2, \tag{7}$$

where $I(0)$ is the intensity of the nth order Bragg peak at time $t=0$; D is the diffusivity at the annealing temperature T and d_{bl} is the bilayer periodicity. The average diffusion length L_d is related to the diffusivity $D(T)$ through the relation $L_d=\sqrt{2D(T)t}$, where t is the annealing time. The diffusivity at the interface of the sample annealed at 300 °C and 400 °C, obtained by XRR measurements, are 2.85×10^{-18} and 1.213×10^{-17} cm^2 sec^{-1}, respectively, with the corresponding diffusion lengths of 17.5 and 36.2 Å, respectively. Using the PNR data we obtained the diffusivities of 4.154×10^{-18} and 1.684×10^{-17} cm^2 sec^{-1} and diffusion lengths of 21.18 and 42.572 Å for the sample annealed at 300 °C and 400 °C, respectively. In spite of the large error bars on the diffusivity and diffusion lengths obtained from XRR and PNR, the values obtained for these parameters match quite closely. We note that in both the experiments, viz., XRR and PNR, we observe an increase in the diffusivity with annealing. In the case of solid-state amorphization reaction in thin films, reaction kinetics slow down.[25] Since the alloying has taken place through the crystalline route in the present sample, diffusion mediated through grain boundaries and defects have helped in rapid alloying. This was also evident in the narrowing of line width in XRD due to the growth in the size of alloy crystallites.

E. Off-specular x-ray reflectivity measurements

The roughness one obtains from specular reflectivity is a convolution of alloying at the interfaces and true roughness.[26] In the present sample, from the specular XRR and NR, we observed that the roughness at the interfaces have gradually increased in the sample, annealed at 300 °C and 400 °C. This can be attributed to rapid alloying at the interfaces. The true roughness can be obtained through measurement of in-plane height-height correlation function at the interfaces by off-specular (or diffuse) reflectivity measurement.[14,23,27] The uncorrelated mean height-height fluctuation gives the true roughness at the interfaces. More importantly, the height-height correlation function also reveals the details of interface morphology at various length scales. In off-specular (or diffuse) reflectivity measurement one measures the reflectivity away from the specular reflectivity condition (angle of incidence=angle of reflection).

Transverse scan is one of the modes of measuring the diffuse scattering from multilayers at grazing incidence.[28] For transverse scans, the scattering angle 2θ is held constant while the angle of incidence, θ_i, and angle of reflection, θ_f, are varied ($\theta_i+\theta_f$=const) by rocking the thin-film sample. If we consider that the momentum transfer in the specular reflectivity is given by q_z, normal to the average plane of a thin film, then in the case of off-specular reflectivity, we get an in-plane component (call it q_x). Typically a narrow specular peak, evident at $q_x=0$, can be separated from the underlying broad diffuse scattering background. In the kinematic limit, a general expression for the diffuse intensity scattered from a single rough surface can be expressed as[14,28–30]

$$I_{diff}\alpha\frac{e^{-q_z^2\sigma^2}}{q_z^2}\int\int dxdy[e^{q_z^2C(x,y)}-1]e^{-i(q_xx+q_yy)}. \tag{8}$$

The in-plane height-height correlation function $C(x,y)$ is usually assumed to be that for a self-affine fractal surface,[14]

$$C(x,y)=\langle\delta z(0)\delta z(x,y)\rangle=\sigma^2\exp\left(-\left[\frac{\sqrt{x^2+y^2}}{\xi}\right]^{2H}\right), \tag{9}$$

where σ is the rms value of the surface roughness, H is the roughness exponent, and ξ is the in-plane correlation length of the roughness. The exponent $0<H<1$ determines the fractal dimension ($D=3-H$) of the interface (i.e., how jagged the interface is; smoother interfaces for larger values of H). The cross section of diffuse scattering from the multilayer system under the distorted wave Born approximation (DWBA) is given by Refs. 28–30. For analyzing the diffused scattering data from the present sample, we have used a Genetic algorithm-based χ^2 minimization program, which uses the formalism developed by Holý *et al.*[30] to obtain the incoherent diffuse scattering cross section for a multilayer sample [see Eq. (16) in Ref. 30].

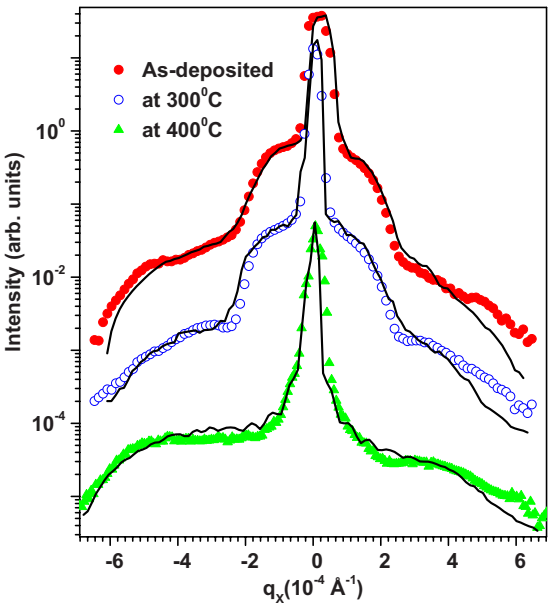

FIG. 7. (Color online) Off-specular x-ray reflectivity measurements from multilayer sample. The measured x-ray rocking scan data for as-deposited multilayer sample (closed circles), sample annealed at 300 °C (open circles), and sample annealed at 400 °C (filled triangle). Continuous lines are fits to corresponding measured data. The data for as-deposited and sample annealed at 300 °C have been shifted for better visualization.

Figure 7(a) displays x-ray transverse scans from as-deposited sample (closed circles) as well as sample annealed at 300 °C (open circles) and 400 °C (open triangle) obtained by rocking the sample about the first-order Bragg-peak reflection. The scans exhibit a resolution limited specular peak and a diffuse component that extends to large values of q_x. The diffuse scattering has been modeled using a height-height correlation function defined in Eq. (9). The interface roughness (σ), Hurst parameter (H), and correlation length (ξ) are the parameters of the fit. For the as-deposited sample we have used two sets of ξ, H, and σ for the two interfaces: Ni on Ti and Ti on Ni. The fit gives average morphology of these interfaces in the multilayer. The two side peaks on both sides of the specular peak in the as-deposited sample [Fig. 7(a)] are the Yoneda wings.[31] Whenever the incident or the reflected angle is equal to the critical angle of Ni or Ti in a rocking scan, these peaks appear. Smearing of these side peaks [Figs. 7(b) and 7(c)] on annealing is also a signature of alloy formation on annealing. We obtained the correlation lengths of 200 and 100 Å for the two interfaces from the fit to the as-deposited sample. The H parameters are 0.13 and 0.35 for the interfaces. After annealing, the Ni-Ti alloy layer is about 50 Å thick with two interfaces with Ni and Ti layers of reduced thickness of ~7 Å. While Hurst parameter of one of the interfaces have increased to 0.17 at the other interface it has increased to 0.42. More importantly we find that the correlation length ξ at both the interfaces increase on annealing. For the Ni interface, ξ rises from 200 Å (as-deposited) to 400 Å (300 °C anneal) and 600 Å after anneal at 400 °C. The same is true for the other interface also. This increase in the correlation length

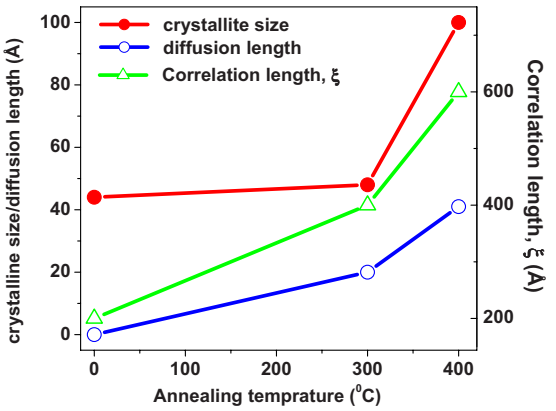

FIG. 8. (Color online) The crystallite size (closed circles), diffusion length (open circles), and in-plane height-height correlation length (open triangles) as a function of annealed temperature.

can be associated with the growth of crystallite size observed in XRD through narrowing of the diffraction line. This is also commensurate with the increase in diffusivity on annealing, which we estimated from Bragg-peak intensities in XRR and PNR.

IV. SUMMARY AND CONCLUSIONS

Rapidly increasing alloy formation as a function of alloying temperature is the most important finding of the present set of studies on Ni/Ti multilayer sample. The as-deposited multilayer had both Ni and Ti layers in crystalline form, and as we annealed the sample at 300 °C and 400 °C, we observe that alloying at the interfaces had progressed through formation of alloy crystallites unlike several studies on Ni/Ti multilayers earlier.[7–9] Interestingly in this crystalline route, the alloy formation has been rapid and the rate of alloy formation increased with annealing. For crystalline alloy layers, rapid alloying is possible through grain boundaries and defects. The major results of this set of studies have been condensed in Fig. 8. We have plotted the crystallite size (obtained from XRD), diffusion length (obtained from XRR and PNR), and the correlation length ξ (obtained from off-specular XRR) together as a function of annealing temperature. These parameters show a remarkable correlation as a function of annealing temperature in the present sample. From PNR data we find that the alloy layers are nonmagnetic in nature and the possibilities are Ni_3Ti and NiTi. From the electron scattering length density obtained from XRR and from the coherent scattering length density obtained from NR, we calculated the volumetric ratio of Ni:Ti equals 2.34:1 in the sample after the second anneal, which endorses the Ni_3Ti composition.

In the present set of studies using XRD, XRR, PNR, and off-specular x-ray reflectivity we have characterized the growth of alloy layers at the interfaces of a Ni/Ti multilayer sample by annealing the sample. We have characterized the structure and morphology of the interface layers in details and shown that if the alloying progresses through formation of crystalline alloy layers, it is increasingly rapid.

[1] F. Mezei, Proc. Soc. Photo-Opt. Instrum. Eng. **83**, 10 (1988).
[2] C. F. Majkrzak and J. L. Wood, SPIE Proceedings on Neutron Optical Devices and Applications (unpublished), p. 1738.
[3] M. Senthil Kumar, P. Böni, and D. Clemens, J. Appl. Phys. **84**, 6940 (1998).
[4] S. Itoh, T. Kamiyama, M. Furusaka, and S. Ikeda, Physica B **241-243**, 79 (1997).
[5] F. E. Wang, W. J. Buehler, and S. J. Pickart, J. Appl. Phys. **36**, 3232 (1965).
[6] T. Lehnert, S. Tixier, P. Böni, and R. Gotthardt, Mater. Sci. Eng., A **273-275**, 713 (1999).
[7] B. M. Clemens, Phys. Rev. B **33**, 7615 (1986).
[8] R. Gupta, M. Gupta, S. K. Kulkarni, S. Kharrazi, A. Gupta, and S. M. Chaudhari, Thin Solid Films **515**, 2213 (2006).
[9] P. Bhatt, A. Sharma, and S. M. Chaudhari, J. Appl. Phys. **97**, 043509 (2005).
[10] F. Klose, Ch. Rehm, D. Nagengast, H. Maletta, and A. Weidinger, Phys. Rev. Lett. **78**, 1150 (1997).
[11] P. Bruno, Phys. Rev. B **52**, 411 (1995).
[12] J. Lekner, *Theory of Reflection of Electromagnetic and Particle Waves* (Martinus Nijhoff, Dordrecht, Netherlands, 1987).
[13] H. Zabel, in *Festkörperprobleme: Advances in Solid State Physics*, edited by U. Rössler (Vieweg, Braunschweig, 1990), Vol. 30, p. 197; T. P. Russell, Annu. Rev. Mater. Sci. **21**, 249 (1991).
[14] S. K. Sinha, E. B. Sirota, S. Garoff, and H. B. Stanley, Phys. Rev. B **38**, 2297 (1988).
[15] S. J. Blundell and J. A. C. Bland, Phys. Rev. B **46**, 3391 (1992).
[16] C. F. Majkrzak, Physica B **173**, 75 (1991).
[17] J. F. Ankner, C. F. Majkrzak, and H. Homma, J. Appl. Phys. **73**, 6436 (1993).
[18] Saibal Basu and Surendra Singh, J. Neutron Res. **14**, 109 (2006).
[19] M. A. Hollanders, B. J. Thijsse, and E. J. Mittemeijer, Phys. Rev. B **42**, 5481 (1990).
[20] V. F. Sears, Neutron News **3**, 26 (1992).
[21] L. Névot and P. Croce, Rev. Phys. Appl. **15**, 761 (1980).
[22] PARRAT32 for multilayer reflectivity calculation and fits, http://www.hmi.de/bensc/instrumentation/instrumente/v6/refl/parratt_en.htm
[23] A. F. Jankowski, Thin Solid Films **220**, 166 (1992).
[24] J. Speakman, P. Rose, J. A. Hunt, N. Cowlam, R. E. Somekh, and A. L. Greer, J. Magn. Magn. Mater. **156**, 411 (1996).
[25] J. C. Barbour, F. W. Saris, M. Nastasi, and J. W. Mayer, Phys. Rev. B **32**, 1363 (1985).
[26] M. Wormington, I. Pape, T. P. A. Hase, B. K. Tanner, and D. K. Bowen, Philos. Mag. Lett. **74**, 211 (1996).
[27] C. Sella, M. Mâaza, M. Miloche, M. Kâabouchi, and R. Krishnan, Surf. Coat. Technol. **60**, 379 (1993).
[28] J.-P. Schlomka, M. Tolan, L. Schwalowsky, O. H. Seeck, J. Stettner, and W. Press, Phys. Rev. B **51**, 2311 (1995).
[29] D. E. Savage, J. Kleiner, N. Schimke, Y.-H. Phang, T. Jankowski, J. Jacobs, R. Kariotis, and M. G. Lagally, J. Appl. Phys. **69**, 1411 (1991).
[30] V. Holý, J. Kuběna, I. Ohlídal, K. Lischka, and W. Plotz, Phys. Rev. B **47**, 15896 (1993).
[31] Y. Yoneda, Phys. Rev. **131**, 2010 (1963).